Running over rough terrain reveals limb control for intrinsic stability

Monica A. Daley[†] and Andrew A. Biewener

Department of Organismic and Evolutionary Biology, Harvard University, 26 Oxford Street, Cambridge, MA 02138

Edited by George N. Somero, Stanford University, Pacific Grove, CA, and approved August 22, 2006 (received for review February 21, 2006)

Legged animals routinely negotiate rough, unpredictable terrain with agility and stability that outmatches any human-built machine. Yet, we know surprisingly little about how animals accomplish this. Current knowledge is largely limited to studies of steady movement. These studies have revealed fundamental mechanisms used by terrestrial animals for steady locomotion. However, it is unclear whether these models provide an appropriate framework for the neuromuscular and mechanical strategies used to achieve dynamic stability over rough terrain. Perturbation experiments shed light on this issue, revealing the interplay between mechanics and neuromuscular control. We measured limb mechanics of helmeted guinea fowl (Numida meleagris) running over an unexpected drop in terrain, comparing their response to predictions of the mass–spring running model. Adjustment of limb contact angle explains 80% of the variation in stance-phase limb loading following the perturbation. Surprisingly, although limb stiffness varies dramatically, it does not influence the response. This result agrees with a mass–spring model, although it differs from previous findings on humans running over surfaces of varying compliance. However, guinea fowl sometimes deviate from mass–spring dynamics through posture-dependent work performance of the limb, leading to substantial energy absorption following the perturbation. This posture-dependent actuation allows the animal to absorb energy and maintain desired velocity on a sudden substrate drop. Thus, posture-dependent work performance of the limb provides inherent velocity control over rough terrain. These findings highlight how simple mechanical models extend to unsteady conditions, providing fundamental insights into neuromuscular control of movement and the design of dynamically stable legged robots and prosthetic devices.

biomechanics | locomotion | motor control | mass–spring model

All legged terrestrial animals use similar basic mechanisms for steady locomotion (1–7). In the stance phase of bouncing gaits, such as hopping and running, kinetic energy (KE) and gravitational potential energy of the body cycle in phase, decreasing during the first half of stance and increasing during the second half (1). Elastic recoil allows this energy to be stored and returned by the elastic structures of the limb (8–11). Consequently, a simple mass–spring model is often used to describe the stance phase dynamics of these gaits. The model consists of a point mass and a linear compression spring (2–4). Despite the simplicity of this model, it appears that humans and animals maintain mass–spring dynamics over a broad range of locomotor conditions by adjusting model parameters: limb contact angle (φ_o), effective limb length (L_o), and leg stiffness (k_{leg}) (4, 5, 12, 13). Nonetheless, the mass–spring model is a conservative system, meaning that the total mechanical energy of the body (E_{com}) does not change over a stride. If energy must be absorbed or produced to change E_{com} (in acceleration or deceleration, for example), the animal must deviate from the simplest spring-like mechanics. Thus, although this model describes well the body mechanics of steady running, it is not yet clear whether it applies to animals running in more complex conditions, including rough or unpredictable terrain.

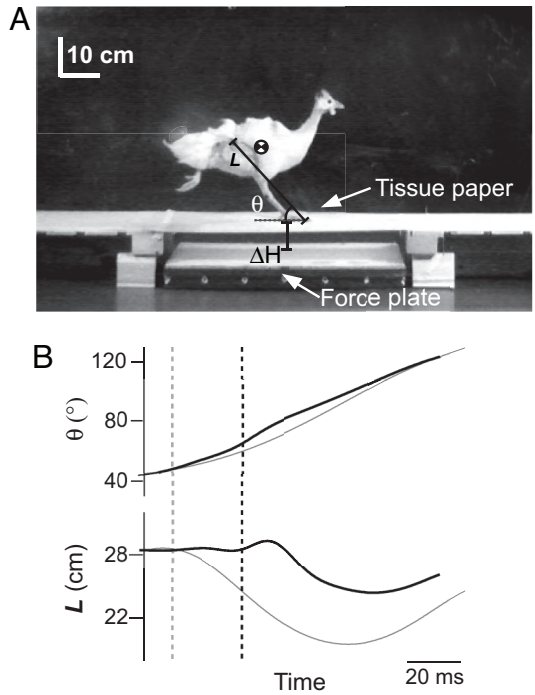

Fig. 1. Limb dynamics following an unexpected perturbation. (*A*) Still frame just prior to an unexpected drop in substrate height. The bird has placed its foot for ground contact on tissue paper that camouflages an 8.5-cm drop in substrate height. Limb length (*L*) and angle relative to horizontal (θ) were measured based on the line between hip and toe. (*B*) Limb angle and limb length over the course of a step (beginning from midswing phase prior) comparing level running (gray traces; C) with perturbed running (black traces; U). Dashed gray line indicates the time of beginning of stance (for C trial) and tissue paper contact (for U trial); dashed black line indicates beginning of stance for U trial. The trial shown here followed the KE_h mode response pattern observed in ref. 14.

We address this issue by using a simple perturbation experiment to investigate limb dynamics following a sudden, unexpected drop in terrain height (ΔH) (Fig. 1*A*). We test the hypothesis that helmeted guinea fowl (*Numida meleagris*) use conservative mass–spring limb mechanics to maintain running stability following this perturbation. The ΔH perturbation results in a 26-ms delay in limb loading relative to that anticipated by the bird (14). In response, the animal can (*i*) rapidly adjust limb position and stiffness to prevent changes in mechanical energy,

Author contributions: M.A.D. and A.A.B. designed research, performed research, analyzed data, and wrote the paper.

The authors declare no conflict of interest.

This article is a PNAS direct submission.

Abbreviations: KE, kinetic energy; COM, center of mass; GRF, ground reaction force.

[†]To whom correspondence should be sent at the present address: Human Neuromechanics Laboratory, Division of Kinesiology, University of Michigan, 401 Washtenaw Avenue, Ann Arbor, MI 48109-2214. E-mail: mdaley@umich.edu.

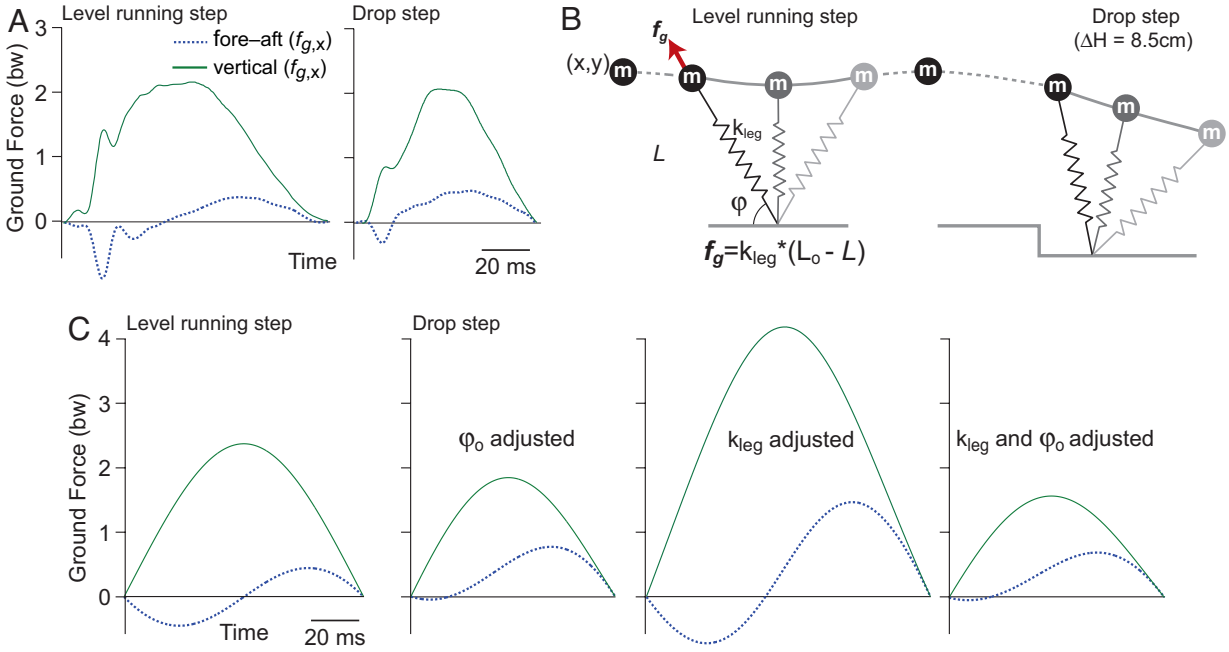

Fig. 2. Comparison of ground forces between model and experiment. (*A*) Ground forces measured during the stance phase of level running and following a drop in terrain (14). (*B*) Schematic of the hypothesized mass–spring model (Eqs. **1**–**3**). (*C*) By adjusting only one parameter, leg contact angle (φ_o), the model predicts ground forces that are similar in magnitude and time course to those measured experimentally. Modeled forces were obtained through numerical integration of Eqs. **1** and **2**.

(*ii*) redistribute energy between gravitational potential energy and KE, or (*iii*) actuate the limb to dissipate energy and change E_{com} (for example, to maintain the same velocity at a lower body height) (14). The animal can accomplish the first two options through conservative spring-like limb mechanics.

This experimental perturbation approach can help reveal the interplay between mechanics and neuromuscular control of running. Similar perturbation approaches have elucidated control strategies for walking, postural stability, lateral stability in hexapedal running, and visuomotor control of flight (e.g., refs. 15–18).

Results

During the time between false floor and ground contact, the limb continues retracting until the foot contacts the lower substrate (Fig. 1*B*). Despite altered limb loading, the leg retracts at a similar average rate as in level running ($P = 0.128$; Fig. 1*B*), although it varies during the perturbation. The delay in ground contact results in a steeper, but more variable, limb contact angle compared with level running ($P = 0.001$; Fig. 1*B* and Fig. 3*B*).

On average, the ground reaction forces measured during the stance phase following the perturbation are approximated well by a conservative mass–spring model (Fig. 2). The magnitude and time-course of ground reaction forces predicted for steady running through numerical simulations using Eqs. **1** and **2** (see *Methods*) are similar to those experimentally measured (Fig. 2). The predicted ground forces for a drop perturbation match those experimentally measured if the model leg spring contact angle (φ_o) is adjusted to the average value measured in perturbation trials. Overall stiffness of the animal's leg (k_{leg}) varies considerably in experimentally perturbed steps (see *Methods*; $k_{leg} = 892 \pm 469$ N·m^{-1}, mean ± SD). However, adjustment of model k_{leg} does not yield an improved match between model and experimental ground forces (Fig. 2*C*).

Consistent with the simulation results, statistical analysis of the experimental data reveals strong correlations between φ_o and a number of stance-phase mechanical variables (Table 1). Both the magnitude of the ground reaction force impulse ($|\mathbf{J}|$) and the duration of contact (T_c) decrease as φ_o approaches vertical ($P < 0.001$ and $P = 0.001$, respectively). Limb stiffness does not significantly correlate with any of the measured stance-phase mechanical variables (Table 1).

The limb as a whole largely preserves spring-like loading characteristics in the step following a terrain drop (Fig. 3 *A* and *B*). Because the linear compression spring in the model is passive and energy-conservative, and resists only axial compression, limb loading is limited by the momentum of the body directed along the leg spring axis during stance (Eq. **3**). Energy storage in the leg spring is limited by the axial kinetic energy at the instant of ground contact. A higher φ_o results in lower axial KE and higher rotational KE (e.g., ref. 19), reducing leg spring loading. Consistent with this, higher measured limb angle (θ_o) is associated with reduced ground forces in perturbation trials (Fig. 3*B*). Additionally, the energy characteristics of the mass–spring model predict 85% of the variation in measured absolute limb work (Fig. 3*C*).

Nonetheless, even during level running, the spring-like dynamics of the limb as a whole arise largely through a balance of positive and negative work among the individual joints, rather

Table 1. Multiple linear regression for effects of K_{leg}, φ_o, and L_o

	Dependent variable			
	$\|\mathbf{J}\|$	ϕ	T_c	$\Delta E_{com}/E_{o,com}$
K_{leg} (X_1)	0.00	0.05	0.00	0.02
φ_o (X_2)	**0.80**	**0.26**	**0.66**	0.06
L_o (X_3)	**0.07**	0.12	0.02	**0.24**
$R^2_{y.1,2,3}$	**0.87**	**0.43**	**0.68**	**0.32**

Dependent variables: $|\mathbf{J}|$, dimensionless impulse magnitude; ϕ, impulse direction; T_c, dimensionless duration of ground contact $[t_c/(L_t)^{1/2}]$; and $\Delta E_{com}/E_{o,com}$, fractional energy change. The value in each cell is the fraction of variance explained by each X variable. The last entry in each column is the R^2 for the full model. Boldface indicates significance at the table-wide $a = 0.05$ level.

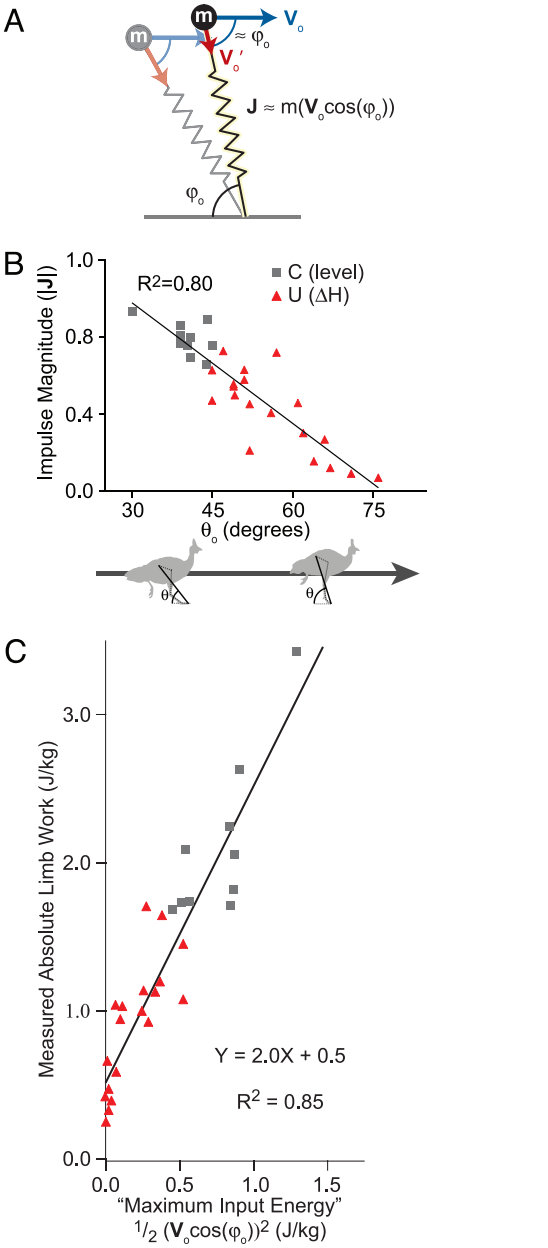

Fig. 3. Limb loading and work following the perturbation are consistent with the mass–spring model. (*A*) Shown is the relationship between leg spring contact angle (φ_o), velocity at contact (V_o), and total ground impulse (**J**) in a mass–spring system (Eq. **3**). If the virtual leg at contact is perpendicular V_o, **J** is zero. (*B*) Measured ground impulse magnitude (|**J**|) (see *Methods*) decreases with increasing limb contact angle θ_o. (*C*) An estimate of mass-specific leg spring energy based on the model (see *Methods*) predicts most of the variation in absolute limb work during stance ($R^2 = 0.85$; $P < 0.0001$).

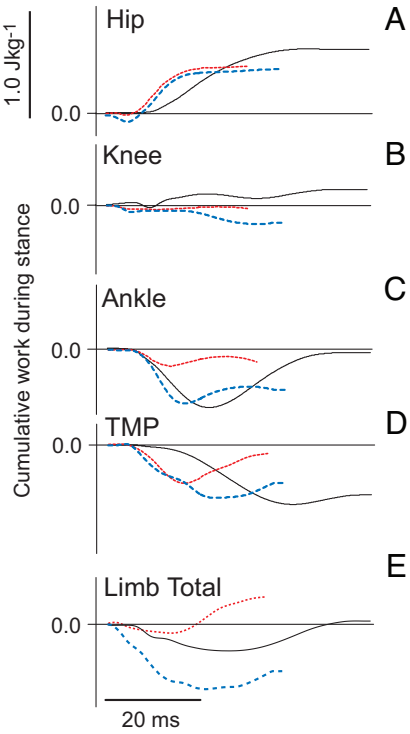

Fig. 4. Joint and limb work during stance. (*A–D*) Hip, knee, ankle, and tarsometatarsophalangeal work over the course of stance, showing a typical level running trial (solid gray) and the two perturbation response modes observed in all individuals: KE_h mode (dotted red) and E_{com} mode (dashed blue) (14). In KE_h mode, the body accelerates forward, whereas in E_{com} mode it does not. (*E*) Total limb work over the course of stance. In level running, the hip produces energy, and the tarsometatarsophalangeal joint absorbs energy, resulting in spring-like energy performance of the whole limb. In KE_h mode, the hip produces energy, and the distal joints act as springs, resulting in net positive limb work. In E_{com} mode, the distal joints absorb more energy than the hip produces, resulting in net negative limb work. The two response modes are associated with different initial limb postures.

than through spring-like patterns of energy storage and return at every joint (Fig. 4). Furthermore, when limb length at the instant of ground contact (L_o) differs from level running, the limb produces or absorbs net energy through a shift of the balance of work among the joints. L_o exhibits a significant inverse linear correlation with net limb work ($R^2 = 0.24$, $P = 0.039$; Table 1 and Fig. 5). This relationship is weak compared with that between φ_o and work magnitude (Fig. 3*C*). However, when divided into high-angle and low-angle trials, the relationship between L_o and ΔE_{com} is more apparent (low-angle trial $R^2 = 0.83$, high-angle trial $R^2 = 0.61$; Fig. 5). Thus, altered limb posture at ground contact is associated with a shift in the balance of work among the joints of the limb, leading to substantial energy production or absorption in the perturbed step.

Discussion

Despite substantial variation in body mechanics, guinea fowl maintain dynamic stability following a sudden drop in terrain that amounts to 40% of leg length (14). This article investigates whether these birds use spring-like limb mechanics to achieve such robust dynamic stability. Adjustment of k_{leg} has often been emphasized as a control strategy for running and hopping (4, 12, 20). However, our experimental results support the theoretical running model of Seyfarth *et al.* (21, 22) that includes automatic adjustment of φ_o to improve stability. In this model, a wide range of k_{leg} values allow stable running, suggesting that k_{leg} is not a critical control parameter for stability (22). Thus, our results highlight a key difference in the control of vertical hopping versus running, which are often treated as mechanical analogues (20, 23). Limb retraction is not required for hopping, but it is an important aspect of running control and strongly influences stabilization dynamics following a step perturbation (as studied here).

Although the guinea fowl maintain spring-like dynamics of the whole body, these dynamics arise through a balance of positive and negative work among the joints, rather than spring-like action at each joint, even in level running (Fig. 4). Consequently, the extent to which the limb preserves spring-like loading

PHYSIOLOGY

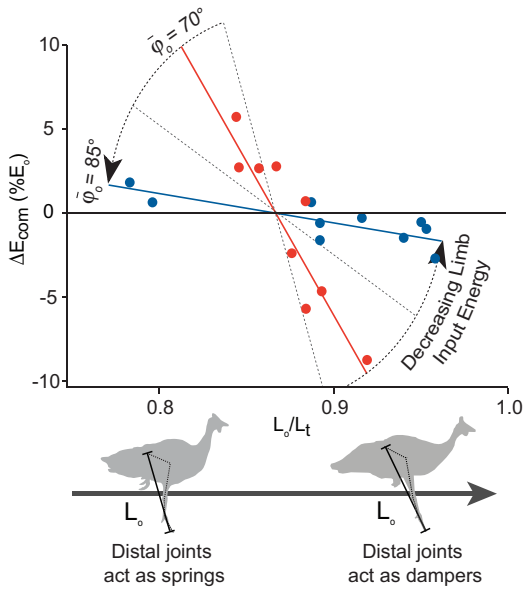

Fig. 5. Posture-dependent limb actuation provides a key stabilizing mechanism. Net energy production of the limb (ΔE_{com}) depends on the interacting effects φ_o and L_o on limb work performance. The magnitude of the work done by the limb depends on φ_o (Fig. 3*C*). However, net energy performance correlates with L_o (Table 1). We have illustrated the interaction between φ_o and L_o by subdividing trials into categories of high angle (blue symbols; mean φ_o = 85°; R^2 = 0.61) and low angle (red symbols; mean φ_o = 70°; R^2 = 0.83). When the limb contacts the ground with a crouched posture, it produces net energy. When the limb contacts the ground with an extended limb posture, it absorbs net energy. Differing limb postures at the instant of ground contact are associated with differing initial knee angle (27).

following a large perturbation is surprising. These results further support the idea that the mass–spring model represents a true control target of the neuromechanical system. Other studies also support this conclusion. Humans maintain mass–spring motion of the body when running or hopping on surfaces of varying compliance, even when the change is unexpected (12, 20, 24). Even on very soft and damped (viscous) surfaces, humans preserve (apparent) spring-like bouncing motion of the center of mass (COM). However, they do so through substantially altered limb function that requires muscular work (25, 26). Together, these findings and the current results suggest that legged animals often use active, actuated mechanisms to return the body to a stable bouncing trajectory following a perturbation.

The current results and a related study on joint mechanics during terrain perturbations (27) suggest that posture-dependent function of the limb results from a proximo-distal gradient in neuromuscular control. We suggest that this neuromuscular control strategy improves stability by allowing limb cycling to remain constant, whereas limb posture, loading, and energy performance are interdependent, rapidly adjusting to uneven terrain.

Despite altered limb loading in perturbed steps, the hip performs similar work as in level running (Fig. 4*A*) (27). Furthermore, the hip largely controls limb retraction, which remains unchanged following the perturbation, suggesting feedforward motor control of the hip extensors (27). The long-fibered parallel architecture of the hip extensor muscles (28) might minimize preflexive effects on contractile performance by the viscoelastic response of muscle to altered loading (29, 30).

Net work produced at the knee remains near zero in perturbed running steps (Fig. 4*B*), although variable knee position at contact appears to reflect variable limb mechanics during the perturbation (27). In contrast to the hip, the knee exhibits variable motion during the tissue breakthrough phase of the perturbation (27). Knee angle is the only joint angle that varies among perturbation trials at the instant of ground contact (27). Altered knee angle at contact is associated with altered θ_o and L_o, and variation in whole-limb energy performance in the stance phase following the perturbation (Fig. 5). Many multiarticular muscles act across the knee, including hip and ankle extensors and hip flexors. Consequently, the variation in knee motion likely reflects altered force balance among the proximal and distal limb muscles following the perturbation.

Unlike the proximal joints, work performance of the distal joints (ankle and tarsometatarsophalangeal) depends on limb loading and limb posture. Both of these joints act as dampers, absorbing energy when the limb contacts the ground with a shallower θ_o and longer L_o, and as springs, absorbing and returning energy when the limb contacts the ground with steeper θ_o and shorter L_o (Fig. 4 *C* and *D*) (27). The greater variation in distal limb muscle performance might result from higher proprioceptive feedback gain (31, 32), greater sensitivity to intrinsic mechanical factors (30), or both. Muscles at distal joints are likely to receive the first proprioceptive information about the interaction between the limb and ground. An *in vivo* study of guinea fowl digital flexor suggests that this distal muscle is sensitive to intrinsic mechanical factors such as length, velocity, and strain history (11). Further study is needed to evaluate how intrinsic muscle-tendon properties and proprioceptive reflex feedback interact to allow rapid adjustment of distal muscle work performance.

Posture-dependent energy performance of the limb provides an important stabilizing mechanism for running over rough terrain. In association with altered L_o relative to control, the limb either absorbs energy, stabilizing the bird at the original velocity, or produces energy, stabilizing the bird at a higher velocity. A mass–spring system can achieve stable running at many different periodic trajectories (33, 34), each characterized by a forward velocity and body apex height (21, 22). In a conservative mass–spring running model, a drop in substrate height results in higher forward velocity upon stabilization because lost gravitational potential energy is redistributed to forward KE. This redistribution alone provides stability, because a mass–spring system is less sensitive to perturbations at higher speeds (21). However, animals must control their velocity in addition to avoiding falls. We previously found that guinea fowl maintain stability but often absorb energy and slow down as they respond to a terrain drop (14). We propose that posture-dependent limb actuation provides a simple mechanism for rapidly switching among running trajectories with different forward velocity, thereby automatically controlling velocity in rough terrain.

What is the benefit of maintaining a spring-like bouncing motion even when the animal does not benefit from the efficiency of a truly elastic system? Control of running through a mass–spring template may simplify control by reducing the complexity of the system to a few controllable limb parameters (6). Recent research suggests that motor control may be modular, generating movement through a limited set of muscle synergies in which subgroups of muscles are activated together in a stereotyped pattern (18, 35). Further, these synergies can correspond to task-level biomechanical functions such as endpoint force or kinematics (18, 36). Muscle synergies are encoded at the level of the spinal cord (37) and may integrate proprioceptive signals into whole-limb information, such as limb length and orientation (38). Similar muscle synergies may exist for running and control parameters such as limb retraction, limb length, and k_{leg}; thereby reducing the complex pattern of muscle activation to a few modules. Activation of each muscle subgroup could be adjusted through proprioceptive feedback at the spinal level, reducing the need for higher-level control and improving response time. Consequently, although the limb does not achieve

truly elastic performance, operation through a mass–spring control template, which might be encoded at the spinal level, could improve stability and simplify the neuromuscular control of running.

Materials and Methods

Animal Training and Data Collection. The data presented here were collected during the same experiments described in a previous study of body COM mechanics (14). Five adult guinea fowl (*N. meleagris*) were trained to run for 1–2 weeks prior to the experiments. The Harvard Institutional Animal Care and Use Committee approved all procedures. In control trials (C), the bird ran across a level runway with a model 9281A forceplate (Kistler, Amherst, NY) at the midpoint. In "unexpected drop" trials (U), the runway was elevated relative to the forceplate, to create a drop in substrate height ($\Delta H = 8.5$ cm), disguised by tissue paper pulled tightly across the gap. Ground reaction force (GRF) and lateral-view high-speed video, using a Motionscope PCI 500 (Redlake, Tucson, AZ), were collected at 5,000 and 250 Hz, respectively.

Ground Reaction Impulse. The vertical (j_v) and fore-aft (j_h) components of the GRF impulse (**J**) were calculated by numerical integration of the instantaneous GRF components (f_v, f_h) over the period of ground contact (t_c), and used to calculate the magnitude ($|\mathbf{J}|$) and angle (ϕ) of the resultant impulse vector (**J**) (14). We estimated the force impulse error due to drift by measuring the change in baseline force over the time period of stance and calculating the impulse that would result from integrating this baseline over time. The error was found to be between 0.0009 and 0.0064 N·s, <1% of the measured ground reaction impulse in the worst case.

Limb Mechanics. Kinematic points located at the middle toe, tarsometatarsophalangeal joint, ankle, knee, hip, synsacrum, and the approximate body COM were digitized and filtered as described in ref. 14. We calculated joint angles, relative limb length (L/L_t, where L is the distance between the hip and toe, and L_t is the sum of all limb segment lengths), limb angle (θ, the angle of the line between hip and toe), and virtual leg spring angle (φ, the angle of the line between the body COM and the force plate center of pressure). Limb angle (θ) averaged $20 \pm 1°$ $< \varphi$ because of the forward position of the body COM relative to the hip. We used inverse dynamics to calculate the external moment and work at each joint over the course of stance. The external moment is the magnitude of the cross product between the instantaneous joint-position vector P and the instantaneous GRF vector F_g. By convention, an extensor moment and an extending angle change were positive. The joint moment and joint angular velocity were multiplied at each time point to obtain instantaneous joint power and numerically integrated to obtain joint work. Using this approach, the value of work at the last time point is the net work done by that joint. We used the same method to calculate the absolute work done at each joint, except that we took the absolute value of joint power prior to integration. All work values were normalized for size by dividing by the bird's body mass.

Average limb stiffness (k_{leg}) was calculated over the duration of limb compression. Limb compression is a decrease in leg length during an increase in GRF. Thus, k_{leg} was the change in force divided by the change in length during limb compression. Note that k_{leg} was not calculated in the same manner as virtual leg spring stiffness in previous studies (4), which assumes mass–spring dynamics. During unsteady behaviors, the limb may not maintain spring-like performance. Our measure of k_{leg} avoids potentially incorrect assumptions about locomotor mechanics during unsteady movement. Nonetheless, if the limb does follow spring-like dynamics, k_{leg} calculated here would equal that obtained through previous approaches.

Mass–Spring Model. We compared limb loading and work performance to the expectations of a simple mass–spring model. The hypothesized mass–spring model is a passive, energy-conservative system that consists of a point mass attached to a mass-less, linear compression spring (3, 4). We numerically simulated this model using the ode45 function in MATLAB release 12 (MathWorks, Natick, MA) with the following equations of motion for the stance phase (Fig. 2*B*) (3):

$$a_x = k_{leg} m^{-1} (L_o - L)\cos(\varphi) \quad [1]$$

$$a_y = k_{leg} m^{-1} (L_o - L)\sin(\varphi) + \mathbf{g}, \quad [2]$$

where m is body mass, φ is the instantaneous angle of the virtual leg spring, k_{leg} is the spring stiffness, L_o is the spring resting length, and L is the spring instantaneous length. This model differs from some recent approaches in that (*i*) no small angle assumptions are made in the equations of motion (19) and (*ii*) gravity is not ignored (39). This approach necessitates a numerical solution but provides a more realistic approximation of guinea fowl behavior. In the flight phase, the body follows a ballistic path. Model parameters (m, k_{leg}, φ, L_o, and body velocity at the instant of contact, V_o) for the level running simulation were obtained from average values for the guinea fowl during the same activity (14, 27). In steps with a drop in terrain, all model parameters were the same as the level running simulation unless specified otherwise.

The leg spring in this model resists loads only in compression along its long axis (it does not resist torque, shear, or axial tension). The total ground reaction force impulse during stance ($\mathbf{J} = \int F_g dt$) follows the equation

$$\mathbf{J} = m\left(\Delta V_x + \Delta V_y + \int \mathbf{g}\sin(\varphi)dt\right). \quad [3]$$

At high speeds the gravitational term is small, and limb loading is limited by the momentum of the body directed along the leg spring axis. Thus, total impulse (**J**) approximately equals $mV_o\cos(\varphi_o)$, assuming that V_o is approximately horizontal (Fig. 3*A*; measured V_o deviated from horizontal by $3 \pm 1°$). Based on this, we estimated a maximum input energy for the leg spring as the axial kinetic energy at the instant of ground contact as $\frac{1}{2}m(V_o\cos(\varphi_o))^2$. For consistency with measured mass-specific limb work values, we normalize for size by canceling the mass (m) term. The total energy stored in the leg spring during loading is equal to the peak force times its change in length (compression). Energy is stored (negative work) until peak force and returned (positive work) as force declines, resulting in absolute limb work equal to twice the energy stored.

Statistical Analysis. All mechanical variables were made dimensionless for statistical analysis by normalizing to body mass (m), the acceleration of gravity (g), and L_t (4). We used simple linear regression to compare measured absolute limb work to that predicted for a mass–spring system. Additionally, to characterize the effect of limb parameters on stance-phase mechanics, a multiple linear regression was used with dimensionless φ_o, L_o, and K_{leg} as independent effects and either $|\mathbf{J}|$, ϕ, T_c, or ΔE_{com} as the dimensionless dependent variable. To account for multiple simultaneous tests, we adjusted the significance level for each test by using the sequential Bonferroni technique. Although the mass–spring model exhibits nonlinearities in many variables, many of the relationships are approximately linear over a biologically relevant range (3). For example, simulation of the mass–spring model over the range of experimentally measured limb contact angles reveals a nonlinear relationship between the limb contact angle and the ground reaction impulse. Nonetheless, the relationship can be approximated with an inverse linear equation, resulting in an R^2 of 0.96.

We thank Pedro Ramirez for animal care and Polly McGuigan, Craig McGowan, Gladys Felix, Jim Usherwood, and Chris Wagner for critical discussion and assistance in data collection. This work was supported by a predoctoral fellowship from the Howard Hughes Medical Institute (to M.A.D.) and by National Institutes of Health Grant AR047679 (to A.A.B.).

1. Cavagna GA, Heglund NC, Taylor CR (1977) *Am J of Physiol* 233:R243–R261.
2. McMahon TA (1985) *J Exp Biol* 115:263–282.
3. Blickhan R (1989) *J Biomech* 22:1217–1227.
4. McMahon TA, Cheng GC (1990) *J Biomech* 23:65–78.
5. Farley CT, Glasheen J, McMahon TA (1993) *J Exp Biol* 185:71–86.
6. Full RJ, Koditschek DE (1999) *J Exp Biol* 202:3325–3332.
7. Dickinson MH, Farley CT, Full RJ, Koehl MAR, Kram R, Lehman S (2000) *Science* 288:100–106.
8. Alexander RM, Bennet-Clark HC (1977) *Nature* 265:114–117.
9. Ker RF, Bennett MB, Bibby SR, Kester RC, Alexander RM (1987) *Nature* 325:147–149.
10. Biewener AA, Baudinette RV (1995) *J Exp Biol* 198:1829–1841.
11. Daley MA, Biewener AA (2003) *J Exp Biol* 206:2941–2958.
12. Ferris DP, Liang K, Farley CT (1999) *J Biomech* 32:787–794.
13. Full RJ, Farley CT (2000) in *Biomechanics and Neural Control of Posture and Movement*, eds Winters JM, Crago PE (Springer, New York), pp 192–205.
14. Daley MA, Usherwood JR, Felix G, Biewener AA (2006) *J Exp Biol* 209:171–187.
15. Gorassini MA, Prochazka A, Hiebert GW, Gauthier MJA (1994) *J Neurophysiol* 71:603–610.
16. Frye MA, Dickinson MH (2001) *Neuron* 32:385–388.
17. Jindrich DL, Full RJ (2002) *J Exp Biol* 205:2803–2823.
18. Ting LH, Macpherson JM (2005) *J Neurophysiol* 93:609–613.
19. Geyer H, Seyfarth A, Blickhan R (2005) *J Theor Biol* 232:315–328.
20. Ferris DP, Farley CT (1997) *J Appl Physiol* 82:15–22.
21. Seyfarth A, Geyer H, Gunther M, Blickhan R (2002) *J Biomech* 35:649–655.
22. Seyfarth A, Geyer H, Herr H (2003) *J Exp Biol* 206:2547–2555.
23. Farley CT, Houdijk HHP, Van Strien C, Louie M (1998) *J Appl Physiol* 85:1044–1055.
24. Moritz CT, Farley CT (2004) *J Appl Physiol* 97:1313–1322.
25. Moritz CT, Farley CT (2003) *Proc R Soc London Ser B* 270:1741–1746.
26. Moritz CT, Farley CT (2005) *J Exp Biol* 208:939–949.
27. Daley MA, Felix G, Biewener AA (2006) *J Exp Biol*, in press.
28. Gatesy SM (1999) *J Morphol* 240:127–142.
29. Loeb GE, Brown IE, Cheng EJ (1999) *Exp Brain Res* 126:1–18.
30. Brown IE, Loeb GE (2000) in *Biomechanics and Neural Control of Posture and Movement*, eds Winters JM, Crago PE (Springer, New York), pp 148–163.
31. Pearson KG, Misiaszek JE (2000) *Brain Res* 883:131–134.
32. Donelan JM, Pearson KG (2004) *J Neurophysiol* 92:2093–2104.
33. Taga G, Yamaguchi Y, Shimizu H (1991) *Biol Cybern* 65:147–159.
34. Full RJ, Kubow T, Schmitt J, Holmes P, Koditschek D (2002) *Integr Compar Biol* 42:149–157.
35. d'Avella A, Bizzi E (2005) *Proc Natl Acad Sci USA* 102:3076–3081.
36. Ting LH, Kautz SA, Brown DA, Zajac FE (1999) *J Neurophysiol* 81:544–551.
37. Saltiel P, Wyler-Duda K, D'Avella A, Tresch MC, Bizzi E (2001) *J Neurophysiol* 85:605–619.
38. Bosco G, Poppele RE, Eian J (2000) *J Neurophysiol* 83:2931–2945.
39. Ghigliazza RM, Altendorfer R, Holmes P, Koditschek D (2005) *SIAM Rev* 47:519–549.